Engineering Structures 174 (2018) 768–777

Contents lists available at ScienceDirect

Engineering Structures

journal homepage: www.elsevier.com/locate/engstruct

Prediction of reinforcement corrosion due to chloride ingress and its effects on serviceability

Karolina Hájková[a,*], Vít Šmilauer[a], Libor Jendele[b], Jan Červenka[b]

[a] Czech Technical University in Prague, Faculty of Civil Engineering, Department of Mechanics, Thákurova 7, 166 29 Prague 6, Czech Republic
[b] Cervenka Consulting s.r.o. Na Hřebenkách 55, 150 00 Prague 5, Czech Republic

ARTICLE INFO

Keywords:
Concrete
Corrosion
Propagation period
Chloride ingress
Serviceability

ABSTRACT

Concrete is the most common man-made material in today's world. Embedded steel reinforcement may corrode due to chloride presence from de-icing salts or salt water, having impact on structural serviceability and life design. The paper presents a chemo-mechanical model covering initiation and propagation periods of chloride steel corrosion, taking into account concrete mix design, supplementary cementitious materials, concrete cover, crack width and environmental conditions. First, a short-term fracture-plastic constitutive model predicts cracking prior to the chloride ingress. Second, 1D model of chloride ingress yields the time of concrete cracking, spalling and the effective steel area. Third, mechanical analysis assesses the load-bearing capacity of a structure in dependence on the state of reinforcement corrosion. Validation includes two load-bearing structures loaded by chlorides; a concrete strut of a prestressed bridge in Prague, Czech Republic and Nougawa bridge, Japan.

1. Introduction

Reinforcement corrosion due to chloride ingress and carbonation are considered to be the most damaging mechanism for reinforced concrete (RC) structures in the world [1]. They generally lead to decreased serviceability and durability, which has a further impact on the life cycle costs and the environment. Chloride ingress is mostly caused by de-icing salts, sea water and salts in coastal areas. Chloride ions diffuse through the binder in concrete and the ingress is controlled by several factors such as environmental boundary conditions, concrete cover thickness, cement type, cement content, water-to-binder ratio (w/b) [2,3].

The classical approach assumes that corrosion starts when the chloride concentration exceeds a critical value in the place of reinforcement [4, Tab. 8.7]. The critical chloride content approaches 0.6% by weight of the binder [5, p. 72]. Other sources give a range of 0.5–0.9% for a tidal and splash zone and 1.6–2.3% for submerged concrete [4, Tab. 8.7].

The initiation period t_i corresponds to no steel corrosion, see Fig. 1. After the initiation period, the propagation period t_p takes place, when the steel reinforcement corrodes and expanding corrosion products are formed. Chlorides often exhibit a pitting corrosion [6]. The times $t_{p,cr}$ and $t_{p,sp}$ in Fig. 1 correspond to the cracking and spalling time of the concrete cover. They are related to corrosion depths $x_{corr,cr}$ and $x_{corr,sp}$ [4].

There are several models predicting the chloride concentration during the ingress [1]. The Mejlbro-Poulsens model [7] assumes the concentration gradient as the driving force, operating on a time-dependent chloride concentration and diffusion coefficients. Kwon's model [8] extends the model for crack effects, which accelerate the ingress [2]. Their role is substantial for traditional cement-based materials, e.g. 0.3 mm cracks may decrease the initiation period approximately five times compared with uncracked concrete [9]. The more realistic ClinConc model decomposes chlorides into free and bound components [10]. This approach leads to a non-linear formulation affected by the binding chloride isotherm [11].

It has been found that the steel corrosion rate depends on the corrosion current density i_{corr}. The models addressing this problem include Liu and Weyer's model [3], models by Alonso [12], Yalçyn and Eugen [13], Vu and Steward [14] or Scott [15] to mention a few.

This article combines Kwon's model [8] for the initiation period with the effect of cracking and Liu and Weyer's model [3] for the propagation period. The amalgamated models predict chloride profiles, the time for cracking and spalling and the decrease of the steel area due to chloride action with consequences for load-bearing capacity and structure reliability.

* Corresponding author.
E-mail addresses: karolina.hajkova@fsv.cvut.cz (K. Hájková), vit.smilauer@fsv.cvut.cz (V. Šmilauer), libor.jendele@cervenka.cz (L. Jendele), jan.cervenka@cervenka.cz (J. Červenka).

https://doi.org/10.1016/j.engstruct.2018.08.006
Received 22 February 2018; Received in revised form 28 July 2018; Accepted 2 August 2018

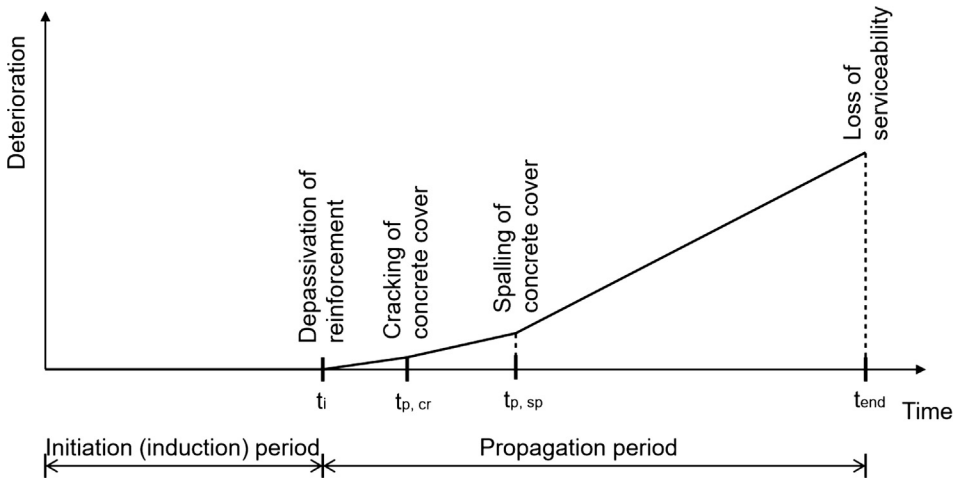

Fig. 1. Initiation and propagation periods.

2. Chemo-mechanical material models

2.1. Models for initiation period

Models for the initiation period assume that steel corrosion starts when the concentration of chloride ion exceeds a critical value [4, Tab. 8.7]. There is an analytical solution for 1D transient ingress with an initially zero chloride content

$$C(x,t) = C_s\left[1-erf\left(\frac{x}{2\sqrt{D_m(t)f(w)t}}\right)\right], \quad f(w) = 31.61w^2 + 4.73w + 1 \tag{1}$$

where C_s is the chloride content at surface (kg of chlorides/kg of a binder), $D_m(t)$ is the mean (averaged) diffusion coefficient at the time t (m^2/s) [2], x is the distance from the surface (m) and $f(w)$ includes acceleration by the crack width w (mm); e.g. a crack width of 0.3 mm increases the mean diffusion coefficient by a factor of 5.26. The preliminary results of the model have been described in detail previously [9]. The solution of Eq. (1) illustrates Fig. 2; a chloride profile with and without cracks from Section 2.1.2.

The instantaneous diffusion coefficient $D(t)$ for chloride ingress is assumed to decrease over the time t according to the power law

$$D(t) = D_{ref}\left(\frac{t_{ref}}{t}\right)^m \tag{2}$$

where m is the decay rate (also called the age factor). The same exponential form was employed in Model Code 2010 [5]. If $m = 0$, a constant value of $D(t) = D_{ref}$ is recovered; such a model was proposed by Collepardi et al. [16]. Nowadays, it has become clear that this assumption is too conservative and is not generally recommended.

The mean diffusion coefficient $D_m(t)$ is obtained by averaging $D(t)$ over the exposure time [17]

$$D_m(t) = \frac{D_{ref}}{1-m}\left(\frac{t_{ref}}{t}\right)^m, \quad t < t_R, \tag{3}$$

$$D_m(t) = D_{ref}\left[1 + \frac{t_R}{t}\left(\frac{m}{1-m}\right)\right]\left(\frac{t_{ref}}{t_R}\right)^m, \quad t \geqslant t_R \tag{4}$$

where t_R is the time, after which the diffusion coefficient remains constant and, which is generally taken as 30 years [18]. t_{ref} corresponds to the time, when the diffusion coefficient was measured. Fig. 3 shows a characteristic evolution of the diffusion coefficient $D(t)$ and $D_m(t)$ through 100 years.

Once crack width changes over time, integration of derived Eq. (1) provides the mean diffusion coefficient $D_m(t)$ as

$$D_{m,w}(t,w) = D_m(t)\int_0^{\overline{w}} 63.22w + 4.73\,\mathrm{d}w \tag{5}$$

2.1.1. Diffusion coefficients for chlorides

The proper determination of diffusion coefficients presents a challenging task, taking into account various cements, concretes, exposure conditions and inverse analysis. The DuraCrete model [4] provides the estimation of the apparent diffusion coefficient from the formula

$$D_a(t) = D_m(t) = k_e k_c D_{Cl}(t_0)\left(\frac{t_0}{t}\right)^m \gamma_{Da} \tag{6}$$

where $k_e \in \langle 0.27, 3.88\rangle$ is the environment factor, $k_c \in \langle 0.79, 2.08\rangle$ is the curing factor, $D_{Cl}(t_0)$ is the measured diffusion coefficient determined at the time t_0, $m \in \langle 0.2, 0.93\rangle$ is the decay rate factor and $\gamma_{Da} \in \langle 1.25, 3.25\rangle$ is the partial factor. In our notation, $D_a(t) = D_m(t)$ and $t_0 = t_{ref}$. Table 1

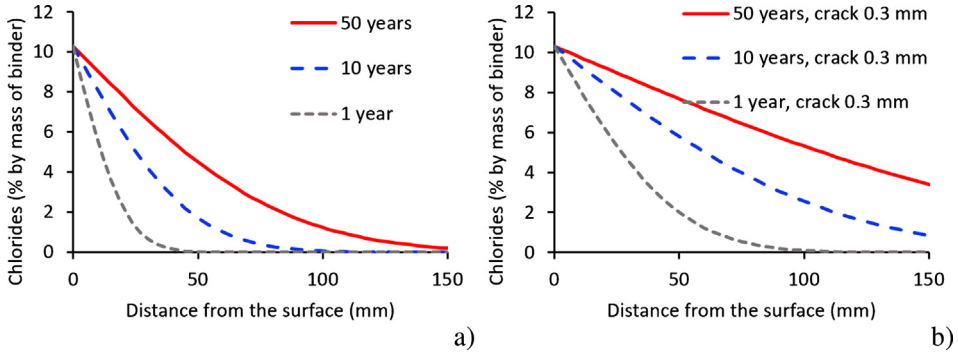

Fig. 2. Effect of cracking on chloride ingress. Chloride profile without cracks (a) and with 0.3 mm crack (b).

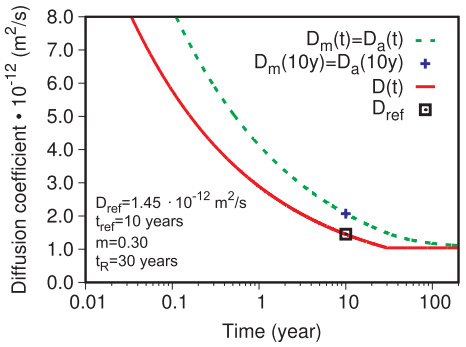

Fig. 3. Evolution of apparent and mean diffusion coefficients.

Table 1
Decay rate factor m for different binder compositions in a spray/splash zone [4, Tab. 8.6].

Binder type	Decay rate factor m (–)
Ordinary Portland Cement (OPC)	0.37
OPC + silica fume	0.39
OPC + slag	0.60
OPC + fly ash	0.93

gives an example of decay rate factors for a spray/splash zone [4, Tab. 8.6].

The experimental data for concretes exposed to a spray zone for 10-years provided more accurate results [19]. The authors stated that the DuraCrete model for a spray zone strongly underestimates the long-term profile, leading to the under-designed life of a structure [19, p. 50]. Fig. 4 summarizes the results from 10-year exposure data in terms of the apparent diffusion coefficient also in dependence of the water-binder ratio. In this particular case, $t_{ref} = 10$ years, m is listed in Table 1, $D_{ref} = (1-m)D_a$, t_R can be assumed as 30 years.

2.1.2. Example of chloride ingress in submerged salt water

Let us consider regular concrete made from ordinary Portland cement, water-to-cement ratio $(w/c) = 0.55$. According to Fig. 4(a), $D_a = 2.07{\cdot}10^{-12}\,\mathrm{m^2\,s^{-1}}$ at $t_{ref} = 10$ years. According to the DuraCrete model [4, Tab. 8.6], the decay rate factor for concrete submerged in sea water corresponds to $m = 0.30$. In such particular case, $D_{ref} = (1-m)D_a = 1.45{\cdot}10^{-12}\,\mathrm{m^2\,s^{-1}}$. Fig. 3 shows the evolution of diffusion coefficients for this particular case.

Let us take a characteristic value $C_s = 10.3\%$ by mass of binder [4, Tab. 8.5], the critical level for corrosion as 1.35% by mass of binder [4, Tab. 8.7] and concrete cover as 100 mm. Table 2 summarizes initiation times according to Eq. (1) with the effect of cracking. It is evident that a macrocrack 0.3 mm decreases the initiation time by almost ten times. The model assumes that the macrocrack width remains constant up to the reinforcement.

2.1.3. Validation of chloride ingress in a spray zone

The validation relies on the data gathered in a Swedish de-icing highway environment where various concrete compositions were exposed to spray/splash conditions [19]. First, let us consider ordinary Portland cement OPC I with $w/c = 0.40$ and $m = 0.37$. The reference diffusion coefficient is calculated from Fig. 4(a) and yields the value $D_a = 0.43{\cdot}10^{-12}\,\mathrm{m^2/s}$ and $D_{ref} = (1-m)D_a = 0.27{\cdot}10^{-12}\,\mathrm{m^2/s}$. Fig. 5(a) shows the measured chloride concentration from two samples, demonstrating also significant variations after a 4.5 year exposure.

Second, the same location and exposure was tested with concrete 95% CEM I + 5% SF, $w/b = 0.40$. The reference diffusion coefficient from Fig. 4(b) yields the value $D_a = 0.33{\cdot}10^{-12}\,\mathrm{m^2/s}$ and $D_{ref} = (1-0.39)D_a = 0.20{\cdot}10^{-12}\,\mathrm{m^2/s}$. Apparently, the silica fume addition decreased D_{ref} by 26% when compared to the previous concrete. It is known that silica fume addition increases the autogenous, drying shrinkage and strength of concrete and such elements are more susceptible to cracking. Fig. 5(b) shows the validated chloride profiles. There is an apparent, small chloride variation in the first 10 mm, signalizing a crack zone. Much better agreement would recover if the boundary condition were shifted 10 mm inside concrete to encounter surface cracking.

3. Models for propagation period

3.1. Corrosion rate during propagation period

The corrosion rate depends on the corrosion current density i_{corr}. The calculation for chloride ingress was formulated by Liu and Weyer's model [3]

$$i_{corr} = 0.926{\cdot}\exp\left[7.98 + 0.7771\ln(1.69{\cdot}C_{M,binder}) - \frac{3006}{T} - 0.000116R_c + 2.24t^{-0.215}\right] \quad (7)$$

where i_{corr} is the corrosion current density ($\mu\mathrm{A/cm^2}$), M_{binder} is the mass of binder ($\mathrm{kg/m^3}$), $C_{M,binder}$ is the total chloride content ($\mathrm{kg/m^3}$ of concrete) at reinforcement determined from 1D non-stationary transport, T is the temperature at the depth of reinforcement (K) and t is the time after initiation (years). R_c is the ohmic resistance of the cover concrete (Ω) [20]

$$R_c = \exp[8.03 - 0.549\ln(1 + 1.69{\cdot}C_{M,binder})] \quad (8)$$

The corrosion rate of reinforcement is based on Faraday's law [21]

$$\dot{x}_{corr}(t) = 0.0116\,i_{corr}(t) \quad (9)$$

where $\dot{x}_{corr}$ is the average corrosion rate in the radial direction (μm/year), i_{corr} is the corrosion current density ($\mu\mathrm{A/cm^2}$) and t is the calculated time after the end of the initiation period (years). By the integration of Eq. (9), the corroded depth is obtained

$$x_{corr}(t) = \int_{t_{ini}}^{t} 0.0116\,i_{corr}(t)R_{corr}\,\mathrm{d}x \quad (10)$$

where x_{corr} is the total amount of corroded steel in the radial direction (mm) and R_{corr} is a parameter depending on the type of corrosion (-). For uniform corrosion (such as carbonation) $R_{corr} = 1$, for pitting corrosion (such as chlorides) $R_{corr} = \langle 2, 4\rangle$ according to [22] or even $R_{corr} = \langle 4, 5.5\rangle$ according to [23]. The effective bar diameter reads

$$d(t) = d_{ini} - \psi 2x_{corr}(t) \quad (11)$$

where $d(t)$ is the evolution of the bar diameter at the time t, d_{ini} is the initial bar diameter (mm), ψ represents an uncertainty factor of the model with a default value of $\psi = 1$ and x_{corr} is the total amount of corroded steel according to Eq. (10).

3.1.1. Cracking of concrete cover

The cracking of concrete can be estimated from the DuraCrete model [4]. The critical penetration depth of corroded steel $x_{corr,cr}$ is formulated as

$$x_{corr,cr} = a_1 + a_2\frac{C}{d_{ini}} + a_3 f_{t,ch} \quad (12)$$

where the parameter $a_1 = 7.44{\cdot}10^{-5}$ m, the parameter $a_2 = 7.30{\cdot}10^{-6}$ m, $a_3 = -1.74{\cdot}10^{-5}$ m/MPa, C is the cover thickness of concrete (m), d_{ini} the initial bar diameter (m), $f_{t,ch}$ is the characteristic splitting tensile strength of concrete (MPa).

3.1.2. Spalling of concrete cover

The critical penetration depth of corroded steel at spalling $x_{corr,sp}$ is calculated from [4] as

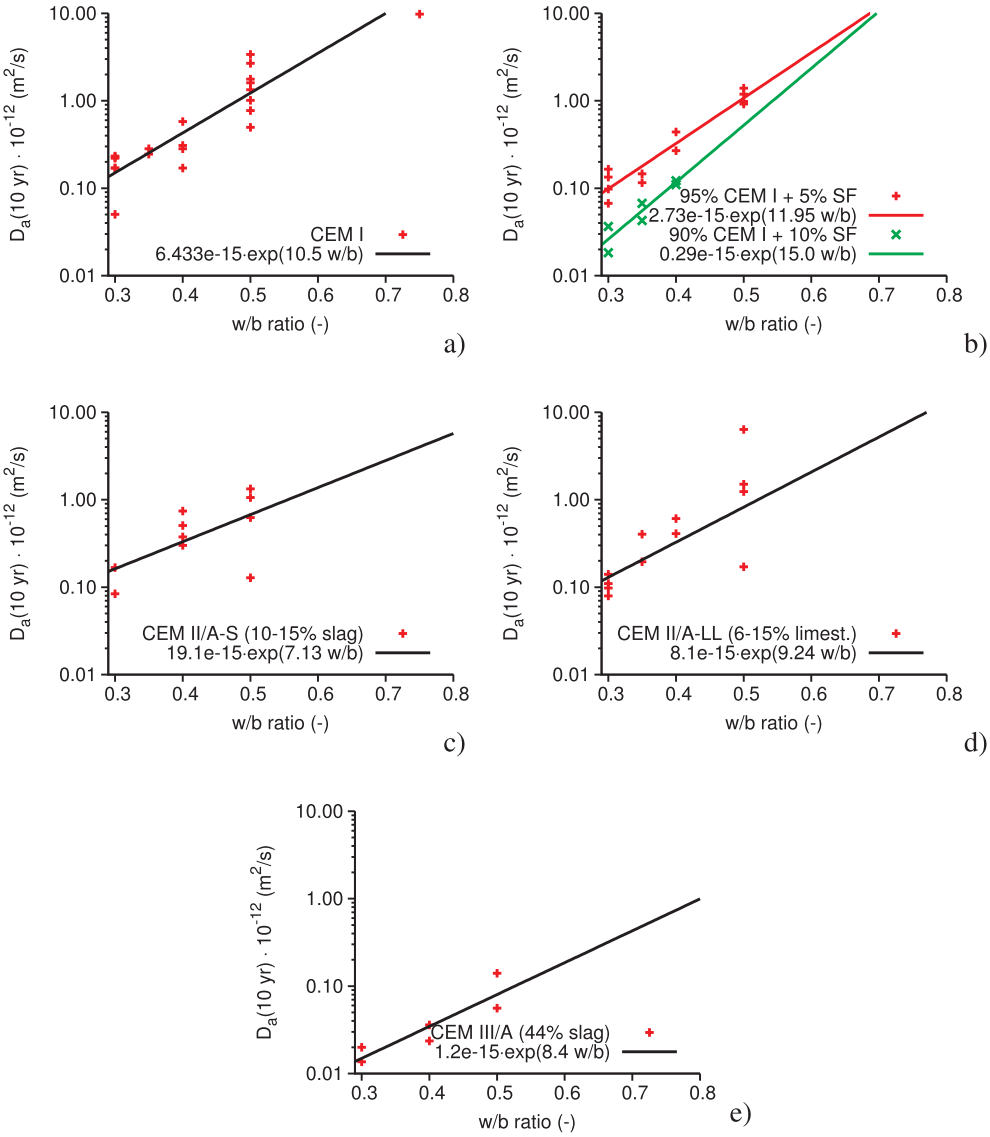

Fig. 4. Apparent diffusion coefficients for different cement types, 10-year exposure of concrete in a spray zone [19].

Table 2
Initiation time for chloride corrosion of submerged concrete, in dependence on original crack width. Cover thickness 100 mm.

Crack width (mm)	Initiation time (years)
0.0	53.8
0.1	23.6
0.2	9.8
0.3	4.7

$$x_{corr,sp} = \frac{w_d - w_0}{b} + x_{corr,cr} \tag{13}$$

where the parameter b depends on the position of the bar (for top reinforcement 8.6 and for bottom 10.4), w_d is the critical crack width for spalling (characteristic value 1 mm), w_0 is the width of the initial crack and $x_{corr,cr}$ the depth of corroded steel at the time of cracking (m).

After the concrete cover spalling, direct steel reinforcement corrosion takes place depending on environment aggressivity. Six corrosivity zones were defined for environments and the values for the first year give [24]; dry indoors C1 ($\leqslant 1.3$), acid/urban inland C2 ($>1.3 \wedge \leqslant 25$), coastal and industrial C3 ($>25 \wedge \leqslant 50$), calm sea-shore C4 ($>50 \wedge \leqslant 80$), surf sea-shore C5($>80 \wedge \leqslant 200$), ocean/off-shore CX ($>200 \wedge \leqslant 700$) µm/year.

3.2. Fracture-plastic model

The nonlinear finite element analyses presented further in this paper are performed with the ATENA software [25] using the combined fracture-plastic model for concrete by Červenka and Papanikolaou [26].

The constitutive model formulation assumes small strains and the strain decomposition into elastic ε_{ij}^e, plastic ε_{ij}^p and fracture ε_{ij}^f components. The stress development is described by the rate equations reflecting progressive damage (concrete cracking) and plastic yielding (concrete crushing)

$$\dot{\sigma}_{ij} = D_{ijkl} \cdot (\dot{\varepsilon}_{kl} - \dot{\varepsilon}_{kl}^p - \dot{\varepsilon}_{kl}^f) \tag{14}$$

Flow rules govern the evolution of plastic and fracturing strains

$$\text{Plastic model: } \varepsilon_{ij}^p = \dot{\lambda}^p \cdot m_{ij}^p, \quad m_{ij}^p = \frac{\partial g^p}{\partial \sigma_{ij}} \tag{15}$$

$$\text{Fracture model: } \varepsilon_{ij}^f = \dot{\lambda}^f \cdot m_{ij}^f, \quad m_{ij}^f = \frac{\partial g^f}{\partial \sigma_{ij}} \tag{16}$$

where $\dot{\lambda}^p$ is the plastic multiplier rate and g^p is the plastic potential

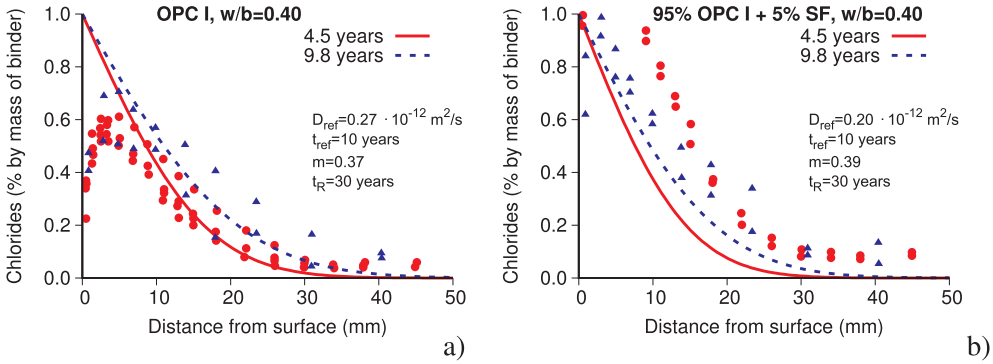

Fig. 5. Validation of chloride ingress on OPC with $w/b = 0.40$ (a) and with the addition of 5% silica fume (b) [19].

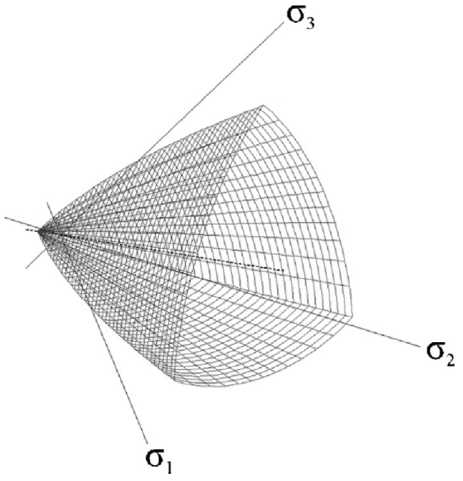

Fig. 6. Visualization of the three-parameter concrete failure criterion; Menetrey and Willam [27].

function, λ^f is the inelastic fracturing multiplier and g^f is the potential defining the direction of inelastic fracturing strains. The multipliers are evaluated from the consistency conditions.

The Menetrey-Willam model [27] is used for the plasticity of concrete in multiaxial stress state in compression, see Fig. 6, with nonlinear hardening in Fig. 7, and linear softening in Fig. 8.

In tension, the Rankine criterion for tensile fracture with exponential softening by Hordijk [28] is used, where w_t stands for the crack width, see Fig. 9.

The stress softening in tension is determined using the crack band approach of Bažant and Oh [29] and, analogically, in compression of Červenka et al. [30]. The crack band as well as the crush band size are adjusted with regard to the crack orientation approach proposed by Červenka and Margoldová [31]. This method is illustrated in Fig. 10

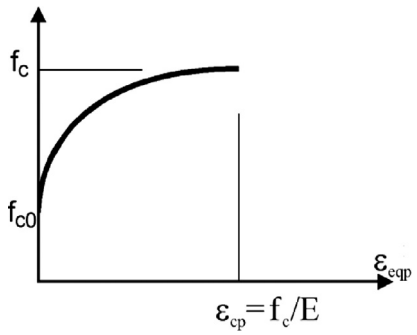

Fig. 7. Hardening law for the concrete plasticity model in compression, E is the Young's modulus.

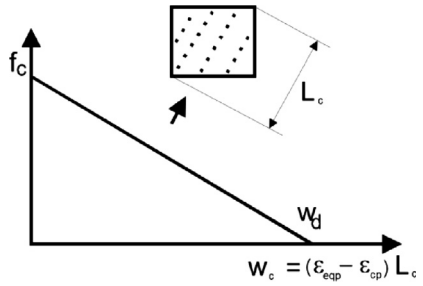

Fig. 8. Softening law for the concrete plasticity model in compression.

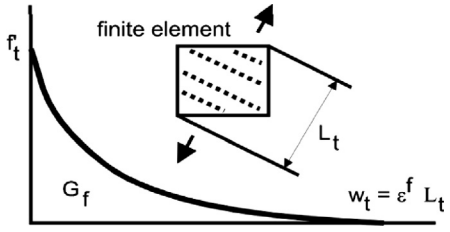

Fig. 9. Crack opening law according to Hordijk [28].

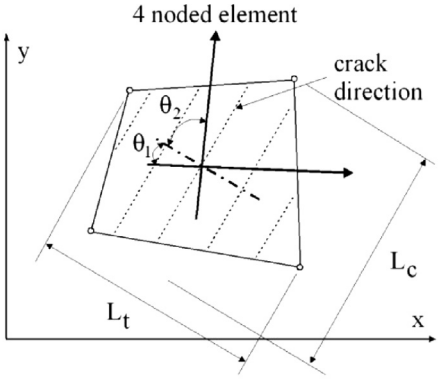

Fig. 10. Crack band formulation.

and described as

$$L_t' = \alpha\gamma L_t \quad \text{and} \quad L_c' = \gamma L_c \tag{17}$$

$$\gamma = 1 + (\gamma_{max} - 1)\frac{\theta}{45}, \quad \theta \in \langle 0;45\rangle, \quad \gamma_{max} = 1.5 \tag{18}$$

The crack angle θ is taken as the average angle between the crack direction and element sides.

The above formulation controls the strain localization accounting for the mesh size and the crack orientation. The parameter α is introduced to cover the localization effect due to the element type as

reported recently in the work of Slobbe et al. [32]. In this study, $\alpha = 1$ is used for low order elements with a 2×2 integration scheme and $\alpha = 0.6$ for quadratic elements with a 3×3 integration scheme.

Some additional features of cracked concrete are included in the model, namely the reduction of compressive strength and shear stiffness degradation, often referred to as a shear retention effect.

The damage of concrete by cracks is reflected according to Bentz et al. [33] in the reduction factor r_c of the compressive strength f_c as

$$\sigma_c = r_c f_c, \quad r_c = \frac{1}{0.8 + 170\varepsilon_1}, \quad r_c^{lim} \leqslant r_c \leqslant 1.0 \tag{19}$$

where ε_1 is the tensile strain normal to the crack. The largest maximal fracturing strain is used for ε_1 and the compressive strength reduction is limited by r_c^{lim}. In this work, $r_c^{lim} = 0.8$ is considered. The shear strength of the cracked surface is also considered according to the modified compression field theory (MCFT) by Bentz et al. [33]

$$\sigma_{ij} \leqslant \frac{0.18\sqrt{f_c'}}{0.31 + \frac{24w}{a_g + 16}}, \quad i \neq j \tag{20}$$

taking into account the crack width w and the aggregate size a_g. Since MCFT does not offer shear stiffness, the authors proposed to relate the shear stiffness K_t^{cr}, oriented tangentially to the crack face, to the normal stiffness K_n^{cr} already defined by the crack opening law

$$K_t^{cr} = s_F K_n^{cr} \tag{21}$$

The normal stiffness comes directly from the tensile softening law in Fig. 9 as

$$K_n^{cr} = f_t(w_t)/w_t \tag{22}$$

This makes the shear stiffness dependent on the crack opening displacement and independent of the mesh size. The scaling factor $s_f = 50$ was used in the presented analyses.

4. Results and discussion

The presented chemo-mechanical model is validated on two engineering structures suffering from chloride ingress, i.e. a concrete strut of a prestressed bridge in Prague, Czech Republic, and Nougawa bridge, Japan. The model is capable of predicting serviceability due to chloride ingress with regards to intrinsic and extrinsic factors.

4.1. Concrete strut of a pre-stressed bridge

The state of a prestressed concrete bridge X-567 in Prague was evaluated after 32 years of service. The total width of the bridge is 12 m, the bridge is built as a precast V-frame with spans of 14 + 36 + 14 m. The reinforced concrete strut marked in Fig. 11 is regularly attacked by chlorides from de-icing salts. Its lower part was analyzed in order to assess reinforcement corrosion due to chloride ingress.

Table 3
Input parameters for chloride ingress.

Parameters	Concrete strut	The Nougawa bridge	Source
D_{ref}	$1.37{\cdot}10^{-7}$ m^2/day	$1.2{\cdot}10^{-7}$ m^2/day	Fig. 4
m_{coeff}	0.37	0.65	Duracrete [4, Tab. 8.6]
C_s	1.7% by mass of binder	4% by mass of binder	Measured values
Cl_{crit}	0.4% by mass of binder	0.6% by mass of binder	Duracrete [4, Tab. 8.7]
$f_{t,ch}$	3.2 MPa	2.6 MPa	Estimated from compressive strength
R_{corr}	2	3	According to [22]
C_{loss}	30 μm/year	35 μm/year	According to category C3 [24]

The concrete of the struts was classified as class C40/50. The estimated composition yields CEM I 42.5 N, 350 kg/m^3 and water content of 180 kg/m^3. The strut is reinforced by stirrups and vertical bars, the latter with a diameter of 32 mm and the concrete cover of 35 mm.

The surface of the strut was exposed to chlorides with the parameters summarized in Table 3. According to the DuraCrete model [4, Tab. 8.6], the decay rate factor for concrete in a tidal and splash zone corresponds to $m = 0.37$. The surfaces are loaded by a measured chloride concentration of 1.7% by mass of binder. The critical level for corrosion is 0.4% per binder as given in EN 206-1. The parameters a_1, a_2, a_3 are estimated from [4]. Corrosion for direct contact with the reinforcement assumes category C3 (coastal and industrial environment) according to [24].

Fig. 12(a) shows the geometry and chloride exposition of the modeled strut. Chloride profiles for the crack width of 0.05 mm are given in Fig. 12(b). It turned out that sound concrete without cracks would yield an unrealistically long initiation time, therefore, hypotheses of crack widths 0, 0.05 and 0.1 mm were tested further.

Those scenarios are demonstrated in Fig. 13. The most realistic assumption favors a crack width of 0.05 mm. In this particular case, the corrosion of reinforcement starts after 18 years, followed by the spalling of the concrete cover after another three years. The concentration of chlorides reaches 0.551% after 32 years at the reinforcement depth while the measured concentration is 0.51% at locations without spalling.

The remaining area of reinforcement reaches 0.944 after 32 years of service. This value is in good agreement with the measured value of 0.95, see Fig. 13(b). Our analysis showed that a crack width of 0.05 mm decreases the initiation time by approximately 1.6 times and the reduction of the reinforcement area is 2.4 times higher compared with sound concrete where reinforcement corrosion would start after 27 years.

Fig. 11. Bridge view with the analyzed strut.

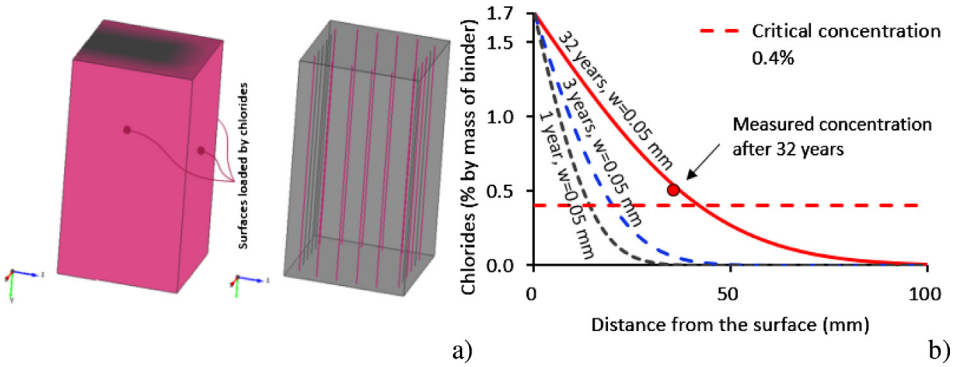

Fig. 12. Geometry (0.6 × 0.75 m) of the bridge strut with a chloride profile and attacked longitudinal reinforcement (a). Chloride profile of the bridge strut for the surface measured concentration of 1.7 by mass of binder and crack width 0.05 mm (b).

4.2. Nougawa bridge, Japan

Nougawa bridge was built in 1930 in a Japanese coastal area. The bridge is a three span reinforced concrete structure with the total length of 131 m. Due to high chloride presence in the air and fast corrosion, the bridge was repaired 30 years after its erection. In 2009 (79 years after the erection), two beams from the bridge were cut out and further investigated, Fig. 14(b).

The beams had stirrups of 9.5 mm, simple longitudinal reinforcement with a diameter of 25.4 mm covered with 47 mm of concrete. The concentration of chlorides and the loss of reinforcement in the mid-spans were experimentally measured and used in the validations.

The calculation consists of three stages, see Fig. 15. First, the bridge was mechanically loaded by the dead weight and the corresponding design life load. Stresses, strains and cracks were calculated in the mechanical part. The following material parameters of the beams were adopted from experimental values; concrete compressive strength of 26 MPa and Young's modulus of 25 GPa at 79 years [34]. Cracks up to 0.3 mm emerged due to the load in the middle span.

The second stage activated the mechano-chemical model with the prediction of the cracking time, spalling time and remaining reinforcement. The surfaces of the beams were exposed to chlorides with the parameters summarized in Table 3. According to the DuraCrete model [4, Tab. 8.6], the decay rate factor was $m = 0.65$ for the atmospheric loading environment. The surfaces were loaded by a measured chloride concentration 4% by mass of binder which fitted the values of a tidal and atmospheric zone in [4, Tab. 8.5]. The critical level for corrosion was 0.6% by mass of binder from [4, Tab. 8.7]. The reinforcement area loss assumed a direct environmental impact for category C3 (coastal and industrial environment) according to [24].

Fig. 16(a) shows the validation of the chloride concentration at point P2 at 79 years of service with measured mid-span values. Fig. 16(b) shows the evolution of the relative reinforcement area at point P2, including the concrete cover restoration. The concrete cover spalled very soon in this case, after 1.5 years. The predicted relative reinforcement area of 63.6% agrees well with the measured value of 62.5%. After refilling the concrete cover, the initiation time becomes 1.88 times longer due to the concrete cover without cracks.

Fig. 17 shows the chloride concentration after 79 years in the place of longitudinal reinforcement. Note that the beams were simply supported on the left side and clamped on the right side to mimic the last span of a continuous beam.

4.2.1. Ultimate limit state analysis of Nougawa bridge's beam

Ultimate limit state analysis (ULS) presents the third and the last modeling stage. The experiments determined load bearing capacity from a cut-out beam. The four-point bending, see Fig. 18(a), recorded the mid-span deflection and applied loading forces. A high level of corrosion and complete destruction of the concrete cover caused that rebar A in Fig. 18(b) detached from the beam. For this reason, this bar was removed in the computational model.

Fig. 19 shows the mesh of the finite element model for ULS analysis. During the four-point bending, tensile fracturing occurred in the middle part and propagated as long as the beam increased its deflection.

Fig. 20(a) evaluates analytically the maximum load from a known, reduced reinforcement area. After the erection, the maximum load corresponded to 340.6 kN and decreased to 193.9 kN at 79 years. Fig. 20(b) shows the ULS simulation at 79 years. The maximum force of 200.9 kN from the simulation (deflection of 0.04 m) drops down to 136 kN due to the rupture of the lower bar layer. No shear failure occurred in the 3D simulation although the stirrups area loss was 55% near the lower surface.

5. Conclusions

The paper presents a chemo-mechanical model for chloride ingress, which allows the simulation of the most important stages during the service life of a steel reinforced concrete structure, i.e. initiation period,

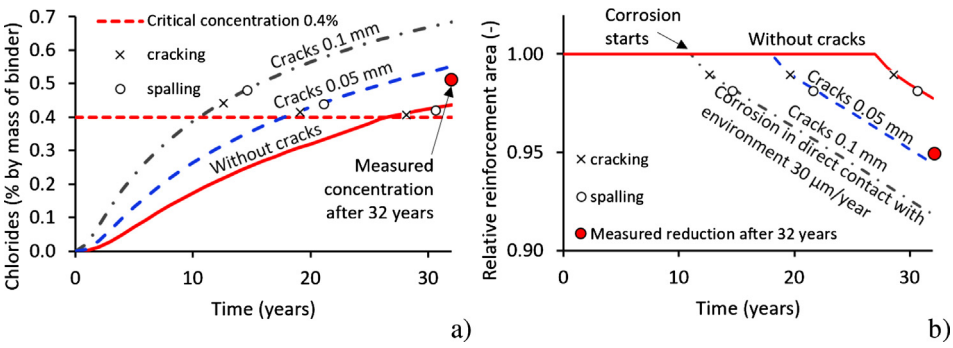

Fig. 13. Chloride concentrations at the reinforcement depth, concrete cover = 35 mm (a). Reduction of the reinforcement area during service life (b).

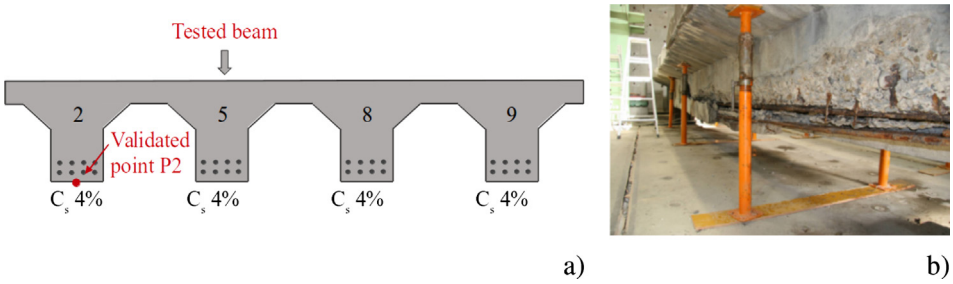

Fig. 14. Cross section of Nougawa bridge (a). Cut-out, validated beam (b) [34].

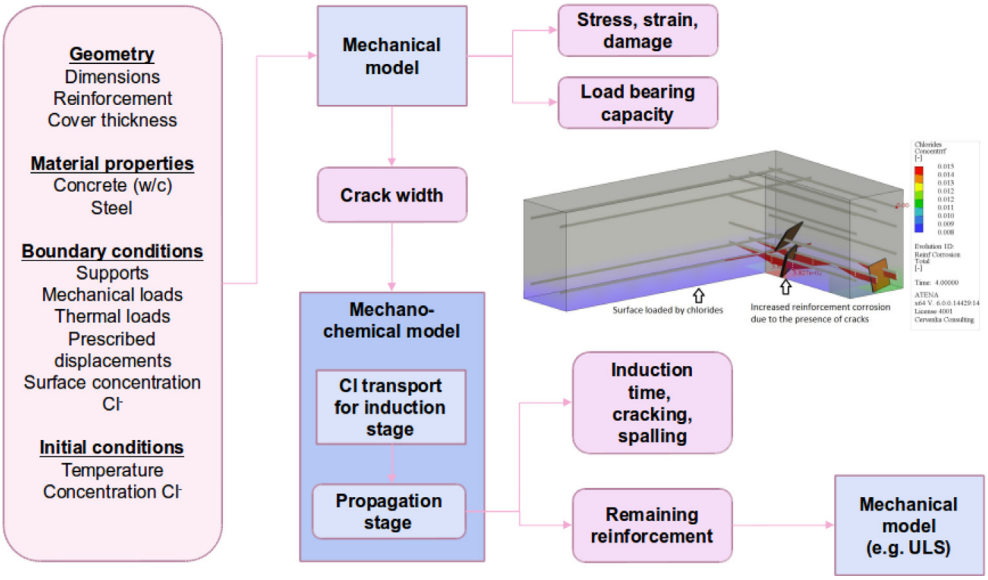

Fig. 15. Modeling workflow for assessing chloride corrosion and load-bearing capacity.

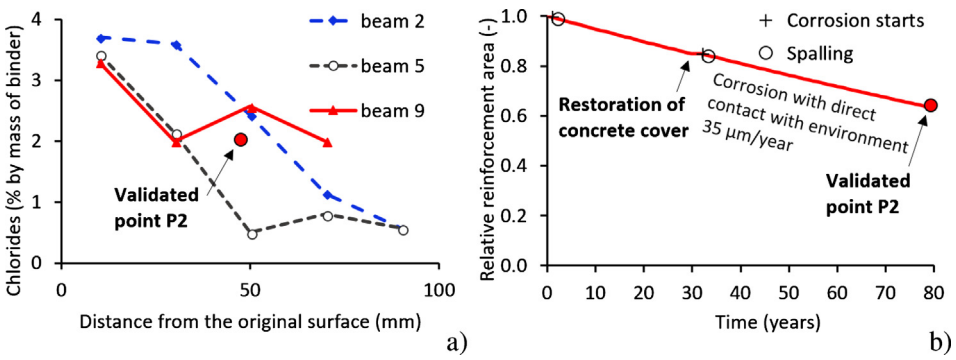

Fig. 16. Profile of chloride concentrations for beams 2, 5, 9 in 79 years (a). Evolution of reinforcement loss at point P2 in 79 years (b). Beam positions are marked in Fig. 14(b).

time of concrete cover cracking, time of concrete cover spalling and direct corrosion of reinforcement. The initiation period is strongly affected by the critical chloride concentration and the concrete cover, concrete diffusivity becomes influenced by the cement type and porosity. The amalgamated models take into account diffusion acceleration due to crack presence contributing to faster chloride ingress.

The validation of a concrete strut demonstrates that a crack width of 0.1 mm decreases the initiation time 2.6 times as compared to uncracked concrete. For this reason, preventing deep macrocrack formation is a crucial factor for durable concrete. This can be facilitated by e.g. proper mix design or fully stressed concrete structures.

The loss of the concrete cover and progressive corrosion still allows the serviceability of several concrete structures. This was demonstrated on Nougawa bridge, Japan, where spalling after 1.5 years and restoration after 30 years kept the bridge in service for 79 years in total. The load-bearing capacity decreased to 56.9% but still kept the bridge in service. Simple diagnostic tools with the help of computational models allow estimating the load-bearing capacity of aging structures.

Several improvements and refinements of the presented models are possible, e.g. chloride binding isotherms, accurate determination of the surface chloride concentration, evolution of chloride diffusivity or a wick action. Chloride ingress is a partially reversible process which can be mitigated by electro-osmosis, reducing the level of chloride concentrations below critical levels.

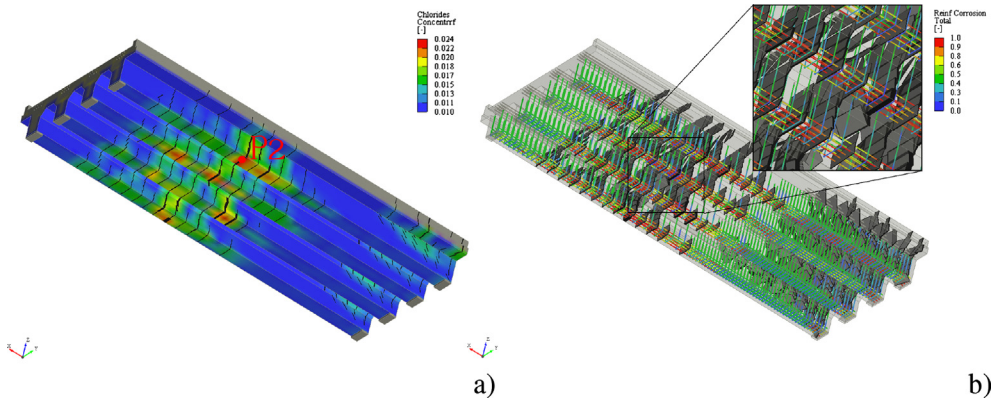

Fig. 17. Concentration of chlorides (by mass of binder) in the place of longitudinal reinforcement after 79 years, validated point P2 (a). Corresponding corrosion of reinforcement after 79 years (2006), the detail shows the mid-span with higher corrosion due to crack presence (b).

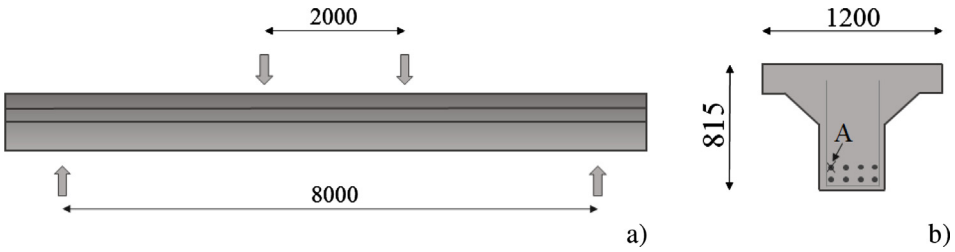

Fig. 18. Experimental setup (a) and cross section of the beam (b) [34].

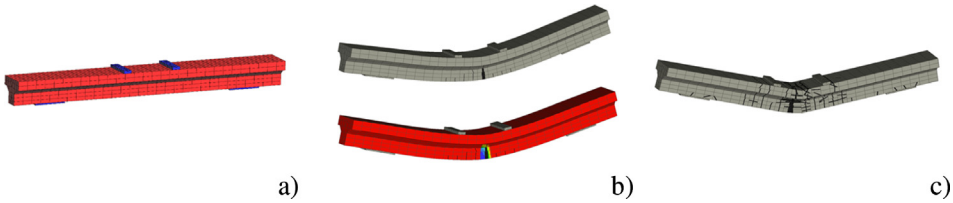

Fig. 19. Simulated beam in four-point bending (a). ULS analysis at 85% of the peak load (b). Maximum deflection at 0.07 m (c).

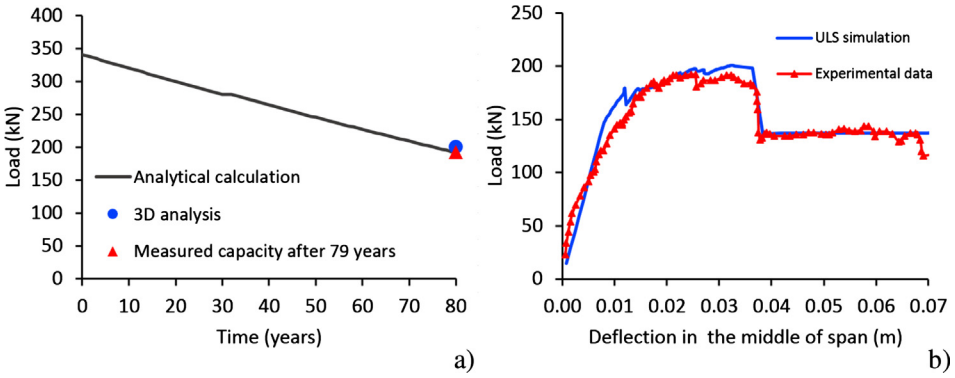

Fig. 20. Analytical calculation of load bearing capacity up to 79 years (a). Evolution of load bearing capacity after 79 years compared with experimental data [34] (b).

Acknowledgement

The authors appreciate the help of V. Junek from Pontex, Ltd., who provided experimental data for a Prague's concrete bridge. We gratefully acknowledge the financial support from the Technology Agency of the Czech Republic under the project TA04031458 and support from Czech Science Foundation under the project 16-20008S.

References

[1] Tang L, Utgenannt P, Boubitsas D. Durability and service life prediction of reinforced concrete structures. J Chin Ceram Soc 2015;43(10):1408–19.
[2] Kwon SJ, Na UJ, Park SS, Jung SH. Service life prediction of concrete wharves with early-aged crack: probabilistic approach for chloride diffusion. Struct Saf 2009;31(1):75–83.
[3] Liu T, Weyers RW. Modeling the dynamic corrosion process in chloride contaminated concrete structures. Cem Concr Res 1998;28(3):365–7.
[4] Muthena A, Andrade C, Nilsson L-O, Edvardsen C, et al. DuraCrete. Final technical report. Tech. rep.; 2000.
[5] Walraven J et al. Model Code 2010. Tech. rep.; Fib 2010.
[6] Duprat F. Reliability of rc beams under chloride-ingress. Constr Build Mater 2007;21(8):1605–16.
[7] Nilsson LO. HETEK: a system for estimation of chloride ingress into concrete: theoretical background. Rapport – Vejdirektoratet, Danish Road Directorate; 1997. URL < https://books.google.cz/books?id = Na7lNAAACAAJ > .

[8] Kwon S-J, Na U-J. Prediction of durability for rc columns with crack and joint under carbonation based on probabilistic approach. Int J Concr Struct Mater 2011;5(1):11–8.
[9] Šmilauer V, Jendele L, Červenka J. Prediction of carbonation and chloride ingress in cracked concrete structures. In: Topping B, editor. Proceedings of the fourteenth international conference on civil, structural and environmental engineering computing; 2013. p. 1–12.
[10] Tang L, Nilsson LO. A numerical method for prediction of chloride penetration into concrete structures. In: The modelling of microstructure and its potential for studying transport properties and durability, vol. 304; 1994. p. 539–52.
[11] Tang L. Chloride transport in concrete: measurement and predictio, Ph.D. thesis, serie 1245. Chalmers University of Technology; 1996.
[12] Alonso C, Andrade C, González JA. Relation between resistivity and corrosion rate of reinforcements in carbonated mortar made with several cement types. Cem Concr Res 1988;18(5):687–98.
[13] Yalçyn H, Ergun M. The prediction of corrosion rates of reinforcing steels in concrete. Cem Concr Res 1996;26(10):1593–9.
[14] Vu T, Steward G. Structural reliability of concrete bridges including improved chloride-induced corrosion models. Cem Concr Res 2000;22(4):313–33.
[15] Scott AN. The influence of binder type and cracking on reinforcing steel corrosion in concrete, Phd thesis. University of Cape Town; 2004.
[16] Collepardi M, Marcialis A, Turriziani R. Penetration of chloride ions into cement pastes and concrete. J Am Ceram Soc 1972;55(10):534–5.
[17] Poulsen E. On a model of chloride ingress into concrete having time dependent diffusion coefficient. In: Nilsson L-O, editor. Chloride penetration into concrete structures, Nordic Mini Seminar, Göteborg; 1993.
[18] Thomas MDA, Bentz D. Life 365 computer program for predicting the service life and life-cycle costs of reinforced concrete structures exposed to chlorides. User Manual (version 1.0.0); 2001.
[19] Luping T, Utgennant P. Chloride ingress and reinforcement corrosion in concrete under de-icing highway environment a study after 10 years field exposure. Sp report 2007:76. SP Sveriges Tekniska Forskningsinstitut; 2007.
[20] Liu Y, Weyers E. Modeling the time-to-corrosion cracking in chloride contaminated reinforced concrete structures. Mater J 1998;95(6):675–80.
[21] Rodriguez J, Ortega LM, Casal J, Diez JM. Corrosion of reinforcement and service life of concrete structures. In: Topping B, editor. Proceedings of international conference on durability of building materials and components; 1996. p. 117–26.
[22] Gonzales JA, Andrade C, Alonso C, Feliu S. Comparison of rates of general corrosion and maximum pitting penetration on concrete embedded steel reinforcement. Cem Concr Res 1995;25(2):257–64.
[23] Darmawan MS, Stewart MG. Effect of pitting corrosion on capacity of prestressing wires. Mag Concr Res 2007;59(2):131–9.
[24] SPEC-NET. Corrosivity zones for steel construction from galvanizers association. ISO 9223 for longer exposure times; 2015.
[25] Červenka V, Červenka J, Jendele L. Atena program documentation, Part 1 theory. Tech. rep. Cervenka Consulting; 2017.
[26] Červenka J, Papanikolaou V. Three dimensional combined fracture-plastic material model for concrete. J Plast 2008;24(12):2192–220.
[27] Menetrey P, Willam KJ. Triaxial failure criterion for concrete and its generalization. ACI Struct J 1995;92(3):311–8.
[28] Hordijk DD. Local approach to fatigue of concrete, Phd thesis. Delft University of Technology; 1991.
[29] Bažant ZP, Oh BH. Crack band theory for fracture of concrete. Mater Struct RILEM Bookser 1983;16(3):155–77.
[30] Červenka J, Červenka V, Laserna S. On finite element modelling of compressive failure in brittle materials. In: Computational modeling of concrete structures, Euro-C 2014, St. Anton, Austria; 2014. p. 273–81.
[31] Červenka V, Margoldová J. Tension stiffening effect in smeared crack model. In: 10th conference of engineering mechanics, Boulder, Colorado; 1995. p. 655–8.
[32] Slobbe AT, Hendriks MAN, Rots JG. Systematic assessment of directional mesh bias with periodic boundary conditions: applied to the crack band model. Eng Fract Mech 2013;109:186–208.
[33] Bentz EC, Vecchio FJ, Collins MP. Simplified modified compression field theory for calculating shear strength of reinforced concrete elements. Struct J 2006;103(4):614–24.
[34] Tanaka Y, Shimomura T, Yamaguchi T. Loading test of rc beam bridge built 80 years ago in japanese coastal area. In: Modelling of corroding concrete structures. RILEM Bookseries, vol. 5; 2010. p. 159–77.